

Potential thermoelectric material $\text{Cs}_2[\text{PdCl}_4]\text{I}_2$: a first-principles study

San-Dong Guo

Department of Physics, School of Sciences, China University of Mining and Technology, Xuzhou 221116, Jiangsu, China

The electronic structures and thermoelectric properties of $\text{Cs}_2[\text{PdCl}_4]\text{I}_2$ are investigated by the first-principles calculations and semiclassical Boltzmann transport theory. Both electron and phonon transport are considered to attain the figure of merit ZT . A modified Becke and Johnson (mBJ) exchange potential, including spin-orbit coupling (SOC), is employed to investigate electronic part of $\text{Cs}_2[\text{PdCl}_4]\text{I}_2$. It is found that SOC has obvious effect on valence bands, producing huge spin-orbital splitting, which leads to remarkable detrimental effect on p-type power factor. However, SOC has a negligible influence on conduction bands, so the n-type power factor hardly change. The temperature dependence of lattice thermal conductivity by assuming an inverse temperature dependence is attained from reported ultralow lattice thermal conductivity of $0.31 \text{ Wm}^{-1}\text{K}^{-1}$ at room temperature. Calculating scattering time τ is challenging, but a hypothetical τ can be adopted to estimate thermoelectric conversion efficiency. The maximal figure of merit ZT is up to about 0.70 and 0.60 with scattering time $\tau=10^{-14}$ s and $\tau=10^{-15}$ s, respectively. These results make us believe that $\text{Cs}_2[\text{PdCl}_4]\text{I}_2$ may be a potential thermoelectric material.

PACS numbers: 72.15.Jf, 71.20.-b, 71.70.Ej, 79.10.-n

Keywords: Spin-orbit coupling; Power factor; Thermal conductivity

I. INTRODUCTION

Thermoelectric materials, which can realize the direct heat to electricity conversion and make essential contributions to the crisis of energy, have attracted a great deal of attention^{1,2}. A good thermoelectric material can be governed by the dimensionless figure of merit $ZT = S^2\sigma T/(\kappa_e + \kappa_L)$, where S , σ , T , κ_e and κ_L are the Seebeck coefficient, electrical conductivity, absolute temperature, the electronic and lattice thermal conductivities, respectively. The high-performance thermoelectric materials should possess high ZT , which requires high power factor ($S^2\sigma$) and low thermal conductivity ($\kappa = \kappa_e + \kappa_L$). The high lattice thermal conductivity is often a fatal disadvantage to gain high ZT value like classic half-Heusler thermoelectric materials³⁻⁶. The lattice thermal conductivity can be reduced by point defects and nanostructuring⁷⁻¹².

However, the ultralow thermal conductivity has been achieved experimentally in SnSe single crystals, and an unprecedented ZT of 2.6 at 923 K has been reported¹³. Theoretically, Atsuto Seko et al. recently discovered 221 materials with very low lattice thermal conductivity, $\text{Cs}_2[\text{PdCl}_4]\text{I}_2$ of which has an electronic band gap of 0.88 eV calculated within generalized gradient approximation (GGA), and ultralow lattice thermal conductivity of $0.31 \text{ Wm}^{-1}\text{K}^{-1}$ at 300K¹⁴. The related electronic structure calculations of $\text{Cs}_2[\text{PdCl}_4]\text{I}_2$ is very less. Recently, Li et al. studied the electronic structures and thermoelectric properties of $\text{Cs}_2[\text{PdCl}_4]\text{I}_2$, and predicted that $\text{Cs}_2[\text{PdCl}_4]\text{I}_2$ is an indirect-band semiconductor with coexistence of several ionic and covalent bonds¹⁵. However, the SOC is neglected, which has important effects on electronic structures for compound containing heavy element like I. The possible ZT has not also been reported.

Here, we report on the thermoelectric properties of

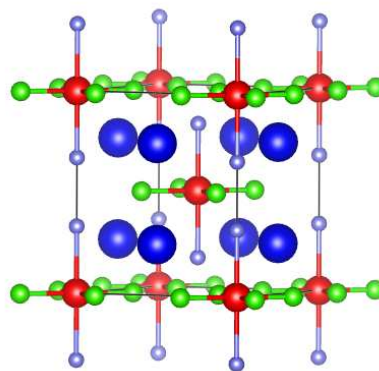
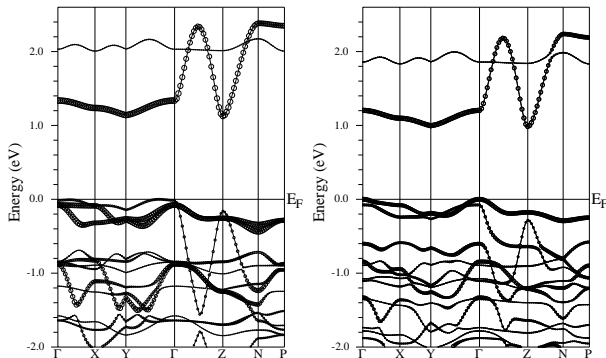


FIG. 1. (Color online) The crystal structure of $\text{Cs}_2[\text{PdCl}_4]\text{I}_2$. The largest balls represent Cs atom, the following is Pd and Cl atoms, and the smallest balls I atoms.

$\text{Cs}_2[\text{PdCl}_4]\text{I}_2$ from a combination of first-principles calculations and semiclassical Boltzmann transport theory. The SOC has been found to be very important for power factor calculations in many thermoelectric materials¹⁶⁻²³, so the SOC is considered in our calculations of electronic part to attain reliable power factor. As is well known, local density approximation (LDA) and GGA underestimate semiconductor energy gaps, and an improved mBJ exchange potential is used to investigate electronic structures of $\text{Cs}_2[\text{PdCl}_4]\text{I}_2$. It is found that SOC has a noteworthy reduced influence on p-type power factor, which can be understood by considering SOC effects on valence bands. The ultralow lattice thermal conductivity is a key factor to attain high ZT , and the corresponding room temperature lattice thermal conductivity of $\text{Cs}_2[\text{PdCl}_4]\text{I}_2$ is only $0.31 \text{ Wm}^{-1}\text{K}^{-1}$ ¹⁴, which can be used to attain temperature dependence of lattice thermal conductivity by assuming an inverse temperature dependence. Finally, the dimensionless thermoelectric figure of merit ZT can be estimated by assuming $\tau=10^{-14}$ s or $\tau=10^{-15}$ s, and

TABLE I. Peak ZT for both n- and p-type with $\tau=10^{-14}$ s and $\tau=10^{-15}$ s, and the corresponding doping concentrations.

T (K)	$\tau=10^{-14}$ s				$\tau=10^{-15}$ s			
	n ($\times 10^{19}\text{cm}^{-3}$)	ZT	p ($\times 10^{19}\text{cm}^{-3}$)	ZT	n ($\times 10^{19}\text{cm}^{-3}$)	ZT	p ($\times 10^{19}\text{cm}^{-3}$)	ZT
600	1.11	0.66	7.34	0.65	5.56	0.40	31.61	0.37
900	1.54	0.71	6.07	0.72	4.26	0.55	25.64	0.52
1200	6.60	0.63	19.07	0.69	7.48	0.58	27.85	0.60
1500	16.83	0.55	55.00	0.66	19.44	0.53	57.75	0.62

FIG. 2. The energy band structures of $\text{Cs}_2[\text{PdCl}_4]\text{I}_2$ using mBJ (Left) and mBJ+SOC (Right), and the dot diameter is proportional to the I atom weight at each k-point.

the ZT can be up to about 0.70 or 0.60 at about 1000 K by the optimized doping.

The rest of the paper is organized as follows. In the next section, we shall describe computational details. In the third section, we shall present the electronic structures and thermoelectric properties of $\text{Cs}_2[\text{PdCl}_4]\text{I}_2$. Finally, we shall give our discussions and conclusion in the fourth section.

II. COMPUTATIONAL DETAIL

The electronic structures of $\text{Cs}_2[\text{PdCl}_4]\text{I}_2$ are performed using a full-potential linearized augmented-plane-waves method within the density functional theory (DFT)²⁴, as implemented in the WIEN2k package²⁵. We employ Tran and Blaha's mBJ exchange potential plus LDA correlation potential for the exchange-correlation potential²⁶, which has been known to produce more accurate band gaps than LDA and GGA. The SOC was included self-consistently^{27–30} due to containing heavy elements, which leads to band splitting, and produces important effects on power factor. We use 5000 k-points in the first Brillouin zone for the self-consistent calculation, make harmonic expansion up to $l_{\text{max}} = 10$ in each of the atomic spheres, and set $R_{\text{mt}} * k_{\text{max}} = 8$. The self-consistent calculations are considered to be converged when the integration of the absolute charge-density dif-

ference between the input and output electron density is less than $0.0001|e|$ per formula unit, where e is the electron charge. Transport calculations, including Seebeck coefficient, electrical conductivity and electronic thermal conductivity, are performed through solving Boltzmann transport equations within the constant scattering time approximation (CSTA) as implemented in BoltzTrap³¹, and reliable results have been obtained for several materials^{32–34}. To obtain accurate transport coefficients, we use 50000 k-points ($36 \times 36 \times 36$ k-point mesh) in the first Brillouin zone for the energy band calculation.

III. MAIN CALCULATED RESULTS AND ANALYSIS

$\text{Cs}_2[\text{PdCl}_4]\text{I}_2$ belongs to tetragonal phase crystal structure with space group $I4/mmm$, which is shown in Figure 1. The experimental lattice parameters ($a=b=8.15$ Å, $c=8.99$ Å)³⁵ are used, and the atomic positions are optimized within GGA. A improved mBJ exchange potential is used to investigate the electronic structures of $\text{Cs}_2[\text{PdCl}_4]\text{I}_2$, which has been proved to be very effective to accurately calculate gaps of all kinds of semiconductors^{26,36,37}. Due to containing heavy element I, it is very crucial for electronic structure calculations to consider SOC. For comparison, the projected energy band structures with both mBJ and mBJ+SOC are shown in Figure 2. Calculated results show that $\text{Cs}_2[\text{PdCl}_4]\text{I}_2$ is a indirect gap semiconductor using both mBJ and mBJ+SOC, and the corresponding gap value is 1.13 eV and 0.99 eV. The mBJ gap value is larger than the reported GGA value of 0.88 eV¹⁴. A noticeable feature of conduction bands is that conduction band minimum (CBM) at Z point and conduction band subminimum at Y point is almost degenerate, namely band convergence^{1,21}, which is benefit for power factor. The projected band structures show that the first three valence bands and first conduction band have obvious I atom character. It is found that SOC has remarkable influence on the valence bands, while has a negligible effect on conduction bands. The SOC leads to giant spin-orbital splitting of the first three valence bands, which produces remarkable effect on power factor of $\text{Cs}_2[\text{PdCl}_4]\text{I}_2$.

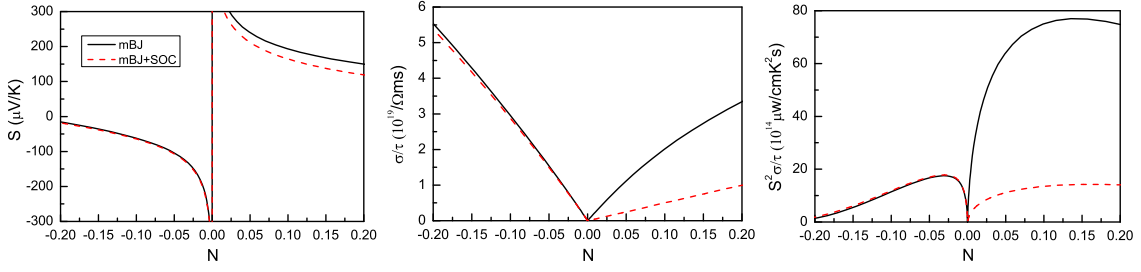


FIG. 3. (Color online) At room temperature (300 K), transport coefficients of $\text{Cs}_2[\text{PdCl}_4]\text{I}_2$ as a function of doping level (N): Seebeck coefficient S , electrical conductivity with respect to scattering time σ/τ and power factor with respect to scattering time $S^2\sigma/\tau$ using mBJ (Black solid lines) and mBJ+SOC (Red dash lines). The doping level (N) implies electrons (minus value) or holes (positive value) per unit cell.

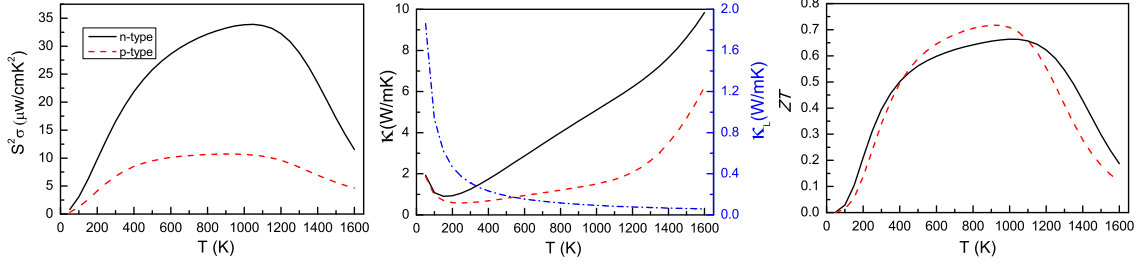


FIG. 4. (Color online) The power factor $S^2\sigma$, thermal conductivities (total thermal conductivity κ and lattice thermal conductivity κ_L) and ZT as a function of temperature with the doping concentration of $5 \times 10^{19} \text{cm}^{-3}$ for n-type and p-type, and the scattering time τ is $1 \times 10^{-14} \text{s}$. The doping concentration equals $3.3518 \times 10^{21} \text{cm}^{-3} \times \text{doping level}$.

The semi-classic transport coefficients are performed using CSTA Boltzmann theory. The doping effects are simulated by shifting the Fermi level within the framework of the rigid band approach, which has been proved to be reasonable in the low doping level^{38–40}. At room temperature, the Seebeck coefficient S , electrical conductivity with respect to scattering time σ/τ and power factor with respect to scattering time $S^2\sigma/\tau$ as a function of doping level using mBJ and mBJ+SOC are shown in Figure 3. The n-type doping (negative doping levels) with the negative Seebeck coefficient can be imitated by shifting Fermi level into the conduction bands. When the Fermi level moves into valence bands, the p-type doping (positive doping levels) with the positive Seebeck coefficient can be achieved. When the SOC is considered, both S and σ/τ are smaller than ones without SOC in p-type doping, while they are nearly the same for n-type. Therefore, $S^2\sigma/\tau$ using mBJ+SOC becomes very small compared to one with mBJ in p-type doping, but it changes almost nothing in n-type doping. At the absence of SOC, p-type best power factor is much larger than n-type one. However, including SOC, n-type best power factor is larger than p-type one. Similar SOC influence on best power factor can be observed in Mg_2Sn ²¹.

The SOC effect on S can be explained by the following formula⁴¹:

$$S = \frac{\pi^2}{3} \left(\frac{k_B^2 T}{e} \right) \left[\frac{1}{n} \frac{dn(E)}{dE} + \frac{1}{\mu} \frac{d\mu(E)}{dE} \right]_{E=E_f} \quad (1)$$

where k_B , e , $n(E)$, $\mu(E)$, E_f are the Boltzmann constant, carrier charge, carrier density at the energy E , mobility, and Fermi energy, respectively. In the valence bands (p-type doping), it is found that $\frac{dn(E)}{dE}$ with mBJ+SOC becomes small with respect to one with mBJ due to remarkable spin-orbit splitting, leading to SOC-reduced S . In conduction bands (n-type doping), $\frac{dn(E)}{dE}$ is almost the same between mBJ and mBJ+SOC, which leads to nearly the same S . Due to σ being proportional to n , the n with SOC is smaller than one without SOC for p-type, leading to reduced σ , and they are almost the same for n-type, producing nearly the same σ .

To attain ZT needs scattering time τ , and calculating τ is challenging from the first-principle calculations. Here, we assume that τ equals $1 \times 10^{-14} \text{s}$. Another key parameter is lattice thermal conductivity κ_L , and the room temperature lattice thermal conductivity has been reported for $0.31 \text{ Wm}^{-1}\text{K}^{-1}$ ¹⁴. An inverse temperature dependence of the lattice thermal conductivity can be found in a large number of thermoelectric materials^{21,22,42,43}. Here, we simply assume that κ_L is proportional to $1/T$ also for $\text{Cs}_2[\text{PdCl}_4]\text{I}_2$. The power factor $S^2\sigma$, total thermal conductivity κ , lattice thermal conductivity κ_L and ZT as a function of temperature with the doping concentration of $5 \times 10^{19} \text{cm}^{-3}$ for n-type and p-type are plotted in Figure 4. The $S^2\sigma$ in both n- and p-type doping firstly increases, and then decreases, when the temperature increases. The total thermal conductivity κ is dominated by the lattice thermal conductivity κ_L in the low tem-

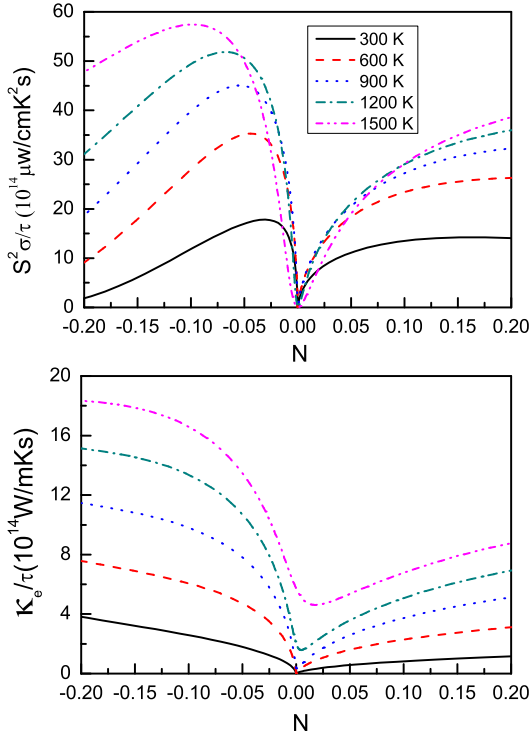


FIG. 5. (Color online) The power factor with respect to scattering time $S^2\sigma/\tau$ and electronic thermal conductivity with respect to scattering time κ_e/τ of $\text{Cs}_2[\text{PdCl}_4]\text{I}_2$ as a function of doping level (N) with temperature being 300, 600, 900, 1200 and 1500 (unit: K) using mBJ+SOC.

perature, but the electronic thermal conductivity κ_e becomes very larger than lattice thermal conductivity κ_L in high temperature region. So, the related temperature of minimum thermal conductivity is very low due to the ultralow lattice thermal conductivity. Both p-type $S^2\sigma$ and κ are smaller than n-type ones in considered temperature range. The ZT has the same trend with $S^2\sigma$ with the increasing temperature. At about 1000 K, the peak ZT of 0.66 is attained in n-type doping. The maximal p-type ZT is 0.72 at about 950 K. The p-type ZT is larger than n-type one from about 400 K to 1100 K.

In order to further understand the thermoelectric properties of $\text{Cs}_2[\text{PdCl}_4]\text{I}_2$, the power factor with respect to scattering time $S^2\sigma/\tau$ and electronic thermal conductivity with respect to scattering time κ_e/τ of $\text{Cs}_2[\text{PdCl}_4]\text{I}_2$ as a function of doping level (N) with temperature being 300, 600, 900, 1200 and 1500 using mBJ+SOC are shown in Figure 5. In the considered doping and temperature range, the $S^2\sigma/\tau$ firstly increases, and then decreases in low doping level with increasing temperature, while it monotonically increases in high doping level. However, κ_e/τ always monotonically increases, when the temperature increases. The corresponding thermoelectric figure of merit ZT with hypothetical $\tau=10^{-14}$ and $\tau=10^{-15}$ s are plotted in Figure 6. As the temperature increases, the ZT has similar trend with $S^2\sigma/\tau$. The peak ZT and

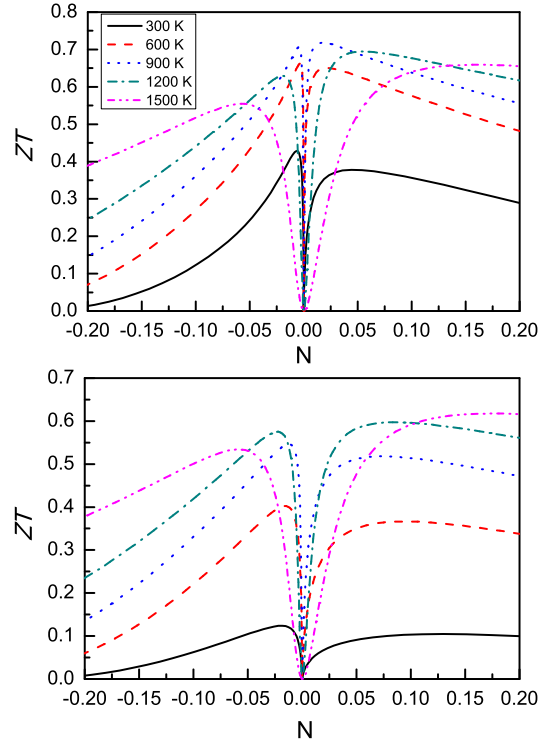


FIG. 6. (Color online) The ZT of $\text{Cs}_2[\text{PdCl}_4]\text{I}_2$ as a function of doping level with temperature being 300, 600, 900, 1200 and 1500 (unit: K), and the scattering time τ is 1×10^{-14} s (Top) and 1×10^{-15} s (Bottom).

corresponding doping concentration at different temperature for both n- and p-type are listed in Table I. It is found that n-type peak ZT has lower doping concentration than p-type one. The doping concentration of peak ZT with $\tau=10^{-15}$ s is larger than one with $\tau=10^{-14}$ s. Calculated results also show that n- and p-type have almost the same maximal ZT , and the maximal ZT with $\tau=10^{-14}$ s and $\tau=10^{-15}$ s is up to about 0.70 and 0.60, respectively.

IV. DISCUSSIONS AND CONCLUSION

The bands of $\text{Cs}_2[\text{PdCl}_4]\text{I}_2$ near the Fermi level are dominated by heavy element I, which produces a giant SOC in the valence bands. The SOC can lift the band degeneracy of valence bands by spin-orbit splitting, especially for the first three valence bands. These SOC effects on valence bands lead to remarkable reduced influence on p-type Seebeck coefficient and electrical conductivity, and further give rise to detrimental influence on power factor. The similar SOC-induced reduced effects on power factor have been observed in many thermoelectric materials^{16,17,21,22}. Therefore, including SOC is very necessary for electronic part of thermoelectric properties of $\text{Cs}_2[\text{PdCl}_4]\text{I}_2$.

In summary, an appropriate exchange-correlation po-

tential mBJ+LDA is chosen to investigate electronic structures and electronic part of thermoelectric properties of $\text{Cs}_2[\text{PdCl}_4]\text{I}_2$, and the SOC is also considered due to containing heavy element I. The strength of SOC effects on valence bands is very huge, especially for the first three valence bands, which leads to obvious reduced effects on p-type power factor. The lattice thermal conductivity κ_L of $\text{Cs}_2[\text{PdCl}_4]\text{I}_2$ is assumed to be proportional to $1/T$, and the κ_L as a function of temperature is attained from the reported room temperature κ_L . Although the scattering time τ is unknown, a hypothetical τ can be employed to estimate possible figure of merit

ZT , which is up to about 0.70 with $\tau=10^{-14}$, and about 0.60 with $\tau=10^{-15}$. Experimentally, it is possible to attain higher ZT than theoretical values. The present work provides a foundation for further experimental studies.

ACKNOWLEDGMENTS

This work is supported by the Fundamental Research Funds for the Central Universities (2015XKMS073). We are grateful to the Advanced Analysis and Computation Center of CUMT for the award of CPU hours to accomplish this work.

-
- ¹ Y. Pei, X. Shi, A. LaLonde, H. Wang, L. Chen and G. J. Snyder, *Nature* **473**, 66 (2011).
 - ² L. E. Bell, *Science* **321**, 1457 (2008).
 - ³ J. R. Sootsman, *Angew. Chem.* **48**, 8616 (2009).
 - ⁴ M. Schwall and B. Balke, *Appl. Phys. Lett.* **98**, 042106 (2011).
 - ⁵ S. Chen and Z. F. Ren, *Mater. Today* **16**, 387 (2013).
 - ⁶ J. Yang, H. M. Li, T. Wu, W. Q. Zhang, L. D. Chen and J. H. Yang, *Adv. Funct. Mater.* **18**, 2880 (2008).
 - ⁷ S. Bhattacharya, M. J. Skove, M. Russell, T. M. Tritt, Y. Xia, V. Ponnambalam, S. J. Poon and N. Thadhani *Phys. Rev. B* **77**, 184203 (2008).
 - ⁸ V. Ponnambalam, P. N. Alboni, J. Edwards, T. M. Tritt, S. R. Culp and S. J. Poon, *J. Appl. Phys.* **103**, 063716 (2008).
 - ⁹ P. F. Qiu, X. Y. Huang, X. H. Chen and L. D. Chen, *J. Appl. Phys.* **106**, 103703 (2009).
 - ¹⁰ N. Shutoh and S. Sakurada, *J. Alloy. Compd.* **389**, 204 (2005).
 - ¹¹ S. Bhattacharya, T. M. Tritt, Y. Xia, V. Ponnambalam, S. J. Poon and N. Thadhani, *Appl. Phys. Lett.* **81**, 43 (2002).
 - ¹² X. Yan, G. Joshi, et al. *Nano Lett.* **11**, 556 (2011).
 - ¹³ L. D. Zhao, S. H. Lo, Y. S. Zhang et al, *Nature* **508**, 373 (2014).
 - ¹⁴ A. Seko, A. Togo, H. Hayashi, K. Tsuda, L. Chaput and I. Tanaka, *Phys. Rev. Lett.* **115**, 205901 (2015).
 - ¹⁵ W. F. Li and G. Yang, *EPL* **113**, 57007 (2016).
 - ¹⁶ K. Kutorasinski, B. Wiendlocha, J. Tobola and S. Kaprzyk, *Phys. Rev. B* **89**, 115205 (2014).
 - ¹⁷ S. D. Guo, *J. Alloy. Compd.* **663**, 128 (2016).
 - ¹⁸ P. Larson, S. D. Mahanti, and M. G. Kanatzidis, *Phys. Rev. B* **61**, 8162 (2000).
 - ¹⁹ T. J. Scheidemantel, C. Ambrosch-Draxl, T. Thonhauser, J. V. Badding, and J. O. Sofo, *Phys. Rev. B* **68**, 125210 (2003).
 - ²⁰ S. J. Youn and A. J. Freeman, *Phys. Rev. B* **63**, 085112 (2001).
 - ²¹ S. D. Guo and J. L. Wang, *RSC Adv.* **6**, 31272 (2016).
 - ²² S. D. Guo, *RSC Adv.* **6**, 47953 (2016).
 - ²³ N. Singh and U. Schwingenschlög, *Phys. Status Solidi RRL* **08**, 805 (2014).
 - ²⁴ P. Hohenberg and W. Kohn, *Phys. Rev.* **136**, B864 (1964); W. Kohn and L. J. Sham, *Phys. Rev.* **140**, A1133 (1965).
 - ²⁵ P. Blaha, K. Schwarz, G. K. H. Madsen, D. Kvasnicka and J. Luitz, WIEN2k, an Augmented Plane Wave + Local Orbitals Program for Calculating Crystal Properties (Karlheinz Schwarz Technische Universität Wien, Austria) 2001, ISBN 3-9501031-1-2
 - ²⁶ F. Tran and P. Blaha, *Phys. Rev. Lett.* **102**, 226401 (2009).
 - ²⁷ A. H. MacDonald, W. E. Pickett and D. D. Koelling, *J. Phys. C* **13**, 2675 (1980).
 - ²⁸ D. J. Singh and L. Nordstrom, *Plane Waves, Pseudopotentials and the LAPW Method*, 2nd Edition (Springer, New York, 2006).
 - ²⁹ J. Kunes, P. Novak, R. Schmid, P. Blaha and K. Schwarz, *Phys. Rev. B* **64**, 153102 (2001).
 - ³⁰ D. D. Koelling, B. N. Harmon, *J. Phys. C: Solid State Phys.* **10**, 3107 (1977).
 - ³¹ G. K. H. Madsen and D. J. Singh, *Comput. Phys. Commun.* **175**, 67 (2006).
 - ³² B. L. Huang and M. Kaviani, *Phys. Rev. B* **77**, 125209 (2008).
 - ³³ L. Q. Xu, Y. P. Zheng and J. C. Zheng, *Phys. Rev. B* **82**, 195102 (2010).
 - ³⁴ J. J. Pulikkotil, D. J. Singh, S. Auluck, M. Saravanan, D. K. Misra, A. Dhar and R. C. Budhani, *Phys. Rev. B* **86**, 155204 (2012).
 - ³⁵ The experimental crystal structure is attained from the Inorganic Crystal Structure Database (ICSD).
 - ³⁶ S. D. Guo, *J. Phys. D: Appl. Phys.* **48**, 445004 (2015).
 - ³⁷ D. Koller, F. Tran and P. Blaha, *Phys. Rev. B* **83**, 195134 (2011).
 - ³⁸ T. J. Scheidemantel, C. Ambrosch-Draxl, T. Thonhauser, J. V. Badding and J. O. Sofo, *Phys. Rev. B* **68**, 125210 (2003).
 - ³⁹ G. K. H. Madsen, *J. Am. Chem. Soc.* **128**, 12140 (2006).
 - ⁴⁰ X. Gao, K. Uehara, D. Klug, S. Patchkovskii, J. Tse and T. Tritt, *Phys. Rev. B* **72**, 125202 (2005).
 - ⁴¹ J. P. Heremans et al., *Science* **321**, 554 (2008).
 - ⁴² D. Parker and D. J. Singh, *Phys. Rev. B* **82**, 035204 (2010).
 - ⁴³ J. J. Pulikkotil et al., *Phys. Rev. B* **86**, 155204 (2012).